Scientia Iranica D (2023) 30(2), 605–617

SCIENTIA IRANICA

Sharif University of Technology
Scientia Iranica
Transactions D: Computer Science & Engineering and Electrical Engineering
http://scientiairanica.sharif.edu

Comparing different configurations for rotary transformer of wound-rotor resolvers

M. Khazaee[a] and F. Tootoonchian[b,*]

a. *School of Advanced Technologies, Iran University of Science and Technology (IUST), Tehran, Iran.*
b. *Electrical Engineering Department, Iran University of Science and Technology (IUST), Tehran, Iran.*

Received 26 March 2021; received in revised form 5 May 2021; accepted 23 August 2021

KEYWORDS
Wound Rotor (WR) Resolver;
Rotary Transformer (RT);
Time Variant Finite Element Method (TVFEM);
Phase shifting error;
Leakage flux;
Total Harmonic Distortion (THD).

Abstract. Wound-rotor resolvers are the oldest and most widely used resolvers. They are two-phase synchronous generators with high-frequency AC excitation. Rotary Transformers (RTs) are used to supply the rotating excitation winding of the resolver. Although RTs offer the benefits of contactless power transmission, the harmonic contents of the secondary voltage, phase shift error between the primary and secondary voltages, and high leakage flux are the main challenges in their applications in the resolvers. The current study aims to examine different configurations of the ferromagnetic core of the RTs to overcome the mentioned problems. To this end, all simulations were done using 3D Time Variant Finite Element Method (TVFEM), and the best configuration was chosen for experimental prototyping and measurements. Close agreement between the simulation and experimental test results approved the performed analysis.

1. Introduction

Among the widely used commercial position sensors are resolvers, optical encoders, and hall effect sensors. Although the last one represents the most cost-effective position sensor [1], it is devoid of acceptable accuracy in high performance motion control systems [2,3]. Optical encoders enjoy high accuracy and acceptable price. However, their sharp accuracy reduction in harsh environments [4,5] is considered their main drawback and for this reason, resolvers are the best choice [6]. Commercial resolvers are divided into two groups: Wound-Rotor (WR) and Variable-Reluctance (VR) resolvers. From the historical point of view, WR resolvers represent the oldest type of resolvers. They can be simply described as the two-phase AC excited synchronous generators built in either brushed or brushless configurations. While the former is extinct now, the latter is still commonly used that requires Rotary Transformer (RT). However, since the employed RT is a non-ideal electrical machine, its usage leads to some difficulties due to leakage flux of the RT and phase shift error between the primary and secondary voltages. The first challenge highlights the necessity of using shields along with the resolver, while the next one causes higher position error of the Resolver-to-Digital Converter (RDC). In fact, commercial RDCs, tracking RDCs, use of the voltage of the primary coil of the RT as the excitation voltage of the resolver, and any phase shift between the real excitation voltage of resolver (the secondary voltage of RT) and primary voltage of the RT increase the chance of error occurring in finding the envelope of the amplitude modulated voltages and consequently, higher position error of the resolver. The mentioned challenges are the main focus of this study. To be specific, different geometrical configurations of RTs were examined to achieve the best structure, pursuing the objective of obtaining minimum phase

*. *Corresponding author.*
E-mail addresses: mehrzadkhazaee13721379@gmail.com (M. Khazaee); tootoonchian@iust.ac.ir (F. Tootoonchian)

doi: 10.24200/sci.2021.57984.5503

shift error and lowest leakage flux. Another solution to the mentioned challenges is the RT omission. Without RT, the rotor of the resolver should had no winding, while VR resolvers had such specifications. Their operation is based on the sinusoidal variation of the air-gap permeance and their excitation winding is transferred to the stator side; hence, they do not need RT [7]. However, they have two main drawbacks: high sensitivity to mechanical tolerances and low accuracy of absolute position measurement [8,9]. Therefore, despite the simple structure of the VR resolvers, the WR ones are the most available sensors in industrial applications.

A number of researches have been conducted on the WR resolvers, while those on the RT ones are scarce and limited. In [10], the individual core of the RT is omitted and instead, the resolver core is used for the RT. Although the proposed structure could reduce the overall volume of the sensor, the flux interference between the RT coils and resolver windings led to the deterioration of the sensor accuracy. In [11], some solutions were proposed to reduce the mentioned flux interference. Then, an analytical model based on the magnetic equivalent circuit was proposed to improve the accuracy of the resolver with no RT core in [12]. However, the accuracy of that resolver after all improvements is lower than that of a similar sensor with the RT core.

In [13], a new method based on the DC-pulse response of the RT primary coil was proposed for identifying the parameters of a rotary transformer. Although the proposed method is verified by experimental measurements, the performance evaluation of the studied RT is out of the scope of this paper. A flat plane RT was proposed in [14] to facilitate feeding the rotor winding of a wound rotor machine. In [15], a cascade RT configuration was suggested for use with Brushless Doubly-Fed Induction Machine (BDFIM). Another configuration called L-form configuration was utilized in [16]. RT with wafer-form winding was developed in [17] for hybrid vehicle applications. In [18], a new configuration with segmented primary core was proposed for supplying circuit of an ultrasonic shaker. The proposed design in [18] was characterized by high leakage inductance and low power loss. Another configuration based on the toothed primary and secondary cores was proposed in [19]. In this configuration, the weight of the employed ferromagnetic material was less than that of conventional RTs in the price of higher leakage inductance. In [20], another configuration with non-magnetic rotor core was presented for RT which made it suitable for high-speed applications. However, due to high electromagnetic air-gap length, the design performance is not acceptable in terms of magnetization current and leakage flux.

Despite proposals of different innovative configurations in the literature, their performance evaluation in terms of phase shift error and amplitude of leakage flux has not been studied yet. In this regard, the current study aims to evaluate and compare the performance of different configurations using finite element method. The values of the outer/inner diameter of the ferromagnetic core, its horizontal length, and number of copper coil turns, and wire diameter of the were kept constant for all configurations. The load and excitation of the studied RTs were also assumed to be identical and finally, the best configuration was chosen for experimental evaluation. Of note, leakage inductance of the windings was calculated and compared to decide on the configuration with the lowest leakage flux.

2. The studied configurations

Six different configurations given in Figure 1(a)–(f) were studied in this paper. RT1 (Figure 1(a)) is referred to as the conventional RT which usually is used with cylindrical resolvers. Flat-plane disk-type RT [14] (Figure 1(b)) is called the RT2. In addition, the L-form RT, called RT3, is given in Figure 1(c) [16]. Figure 1(d) shows the segmented primary core RT, i.e., RT4 [18]. Figure 1(e) shows the RT with toothed cores, called RT5 [19]. Finally, Figure 1(f) shows the RT6 which is equipped with sandwiched winding [20]. All the studied configurations were designed to have a constant volume in constant outer diameter and constant overall length. Other geometrical dimensions of the RTs are presented in Table 1.

Each of the primary and secondary coils of all RTs has 100-turn conductors. The primary coil is fed using 5 V, 4 kHz sinusoidal voltage, as shown in Figure 2.

The design steps for a rotary transformer are the same as those for the high-frequency transformers. The common design method for such transformers is the area product, i.e., transformer window area times the cross-sectional area. However, the main difference between the RT design and that of common High-Frequency Transformers (HFTs) is referred to as the selecting core. In the HFT design, the core dimensions are determined using the area product and then, the closest dimension to the calculated one is selected from the available commercial cores. However, given that the employed cores for RTs have no standard, the

Table 1. Geometrical dimensions of the studied RTs.

Description	Unit	Value
Outer/inner diameter of RTs	mm	42.7/32
Number of primary/secondary coils	–	100/100
Air-gap length	mm	0.35
Horizontal length of the core	mm	8.5
Vertical core length	mm	5

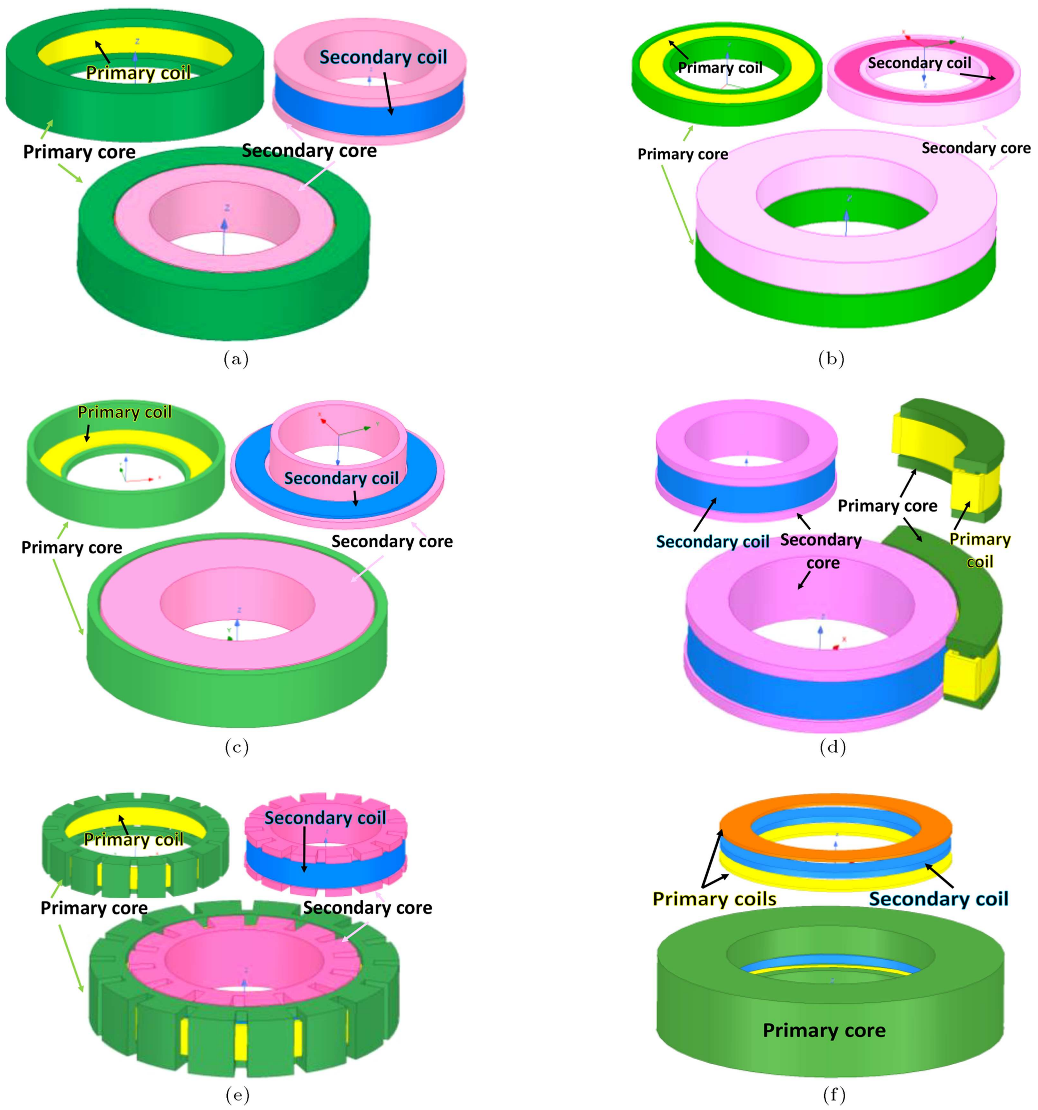

Figure 1. The studied configurations for RT: (a) RT1: Conventional RT, (b) RT2: Flat-plane, disk type RT [14], (c) RT3: L-form RT [16], (d) RT4: segmented primary core RT [18], (e) RT5: with toothed cores [19], and (f) RT6: equipped with sandwiched winding [20].

main dimensions must be calculated according to the calculated area product. The design process for the RTs is shown in Figure 3 according to which the first step in the design is to choose the ferromagnetic martial

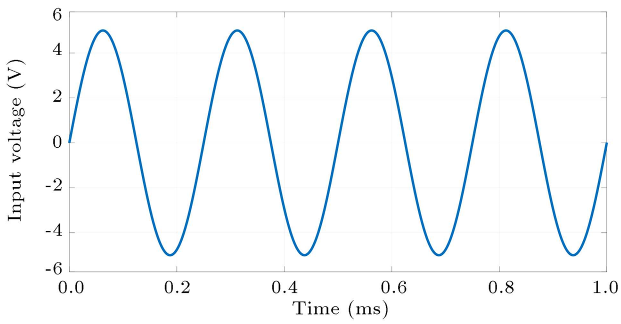

Figure 2. The employed sinusoidal voltage as the excitation of primary coil.

(maximum flux density of the core, B_m), frequency (f), primary nominal voltage (V_1), current density (J_w), wave form factor (K_f), and the space factor (K_u). Then, the area product can be calculated as:

$$A_p = A_c.A_w = \frac{V_1 I_1 + V_2 I_2}{K_f.K_u.f.B_m.J_w}, \tag{1}$$

where A_c is the appropriate core size and A_w is the window area of the transformer. The core dimensions should be determined according to the selected geometry, maximum speed, and allowed volume of the RT. The next step is to calculate the turn numbers considering the nominal voltage. The diameter of the copper conductors is determined, considering the nominal current and the current density. Next, once the RT performance is approved, its electrical and mechanical parameters can be calculated.

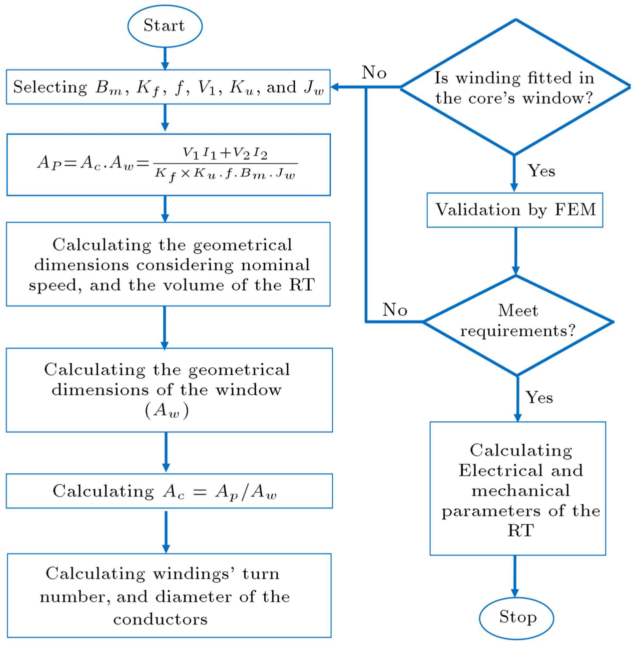

Figure 3. The flowchart of the RT design.

Let us consider the flux linkage of the primary (λ_1) and secondary (λ_2) coils as:

$$\lambda_1 = N_1 \varphi_1 = N_1(\varphi_{l1} + \varphi_m), \tag{2}$$

$$\lambda_2 = N_2 \varphi_2 = N_2(\varphi_{l2} + \varphi_m), \tag{3}$$

where N_1/N_2 is the turn number of the primary/secondary coils, φ_1/φ_2 the total flux of primary/secondary coils, $\frac{\varphi_{l1}}{\varphi_{l2}}$ the leakage flux of primary/secondary coils, and φ_m the mutual flux.

Based on the relation among the Magnetomotive force (MMF), magnetic flux (φ), and permeance (P), we have:

$$\varphi = P \times MMF. \tag{4}$$

Upon substituting the permeance relation (Eq. (3)) into the flux linkage expressions (Eqs. (2) and (3)), we have:

$$\begin{aligned}\lambda_1 &= N_1\{P_{l1}(N_1 i_1) + P_m(N_1 i_1 + N_2 i_2)\}\\ &= ({N_1}^2 P_{l1} + {N_1}^2 P_m) i_1 + N_1 N_2 P_m i_2\\ &= \underbrace{(L_{l1} + L_{m1})}_{L_{11}} i_1 + L_{12} i_2,\end{aligned} \tag{5}$$

$$\begin{aligned}\lambda_2 &= N_2\{P_{l2}(N_2 i_2) + P_m(N_1 i_1 + N_2 i_2)\}\\ &= ({N_2}^2 P_{l2} + {N_2}^2 P_m) i_1 + N_1 N_2 P_m i_1\\ &= L_{21} i_1 + \underbrace{(L_{l2} + L_{m2})}_{L_{22}} i_2,\end{aligned} \tag{6}$$

where L_{l1} and L_{l2} are the leakage inductances of the coils; L_{m1} and L_{m2} are the magnetizing inductances, L_{11} and L_{22} the self-inductance of the windings; and L_{12} and L_{21} the mutual inductances between them. The leakage inductance of the coils can be calculated as:

$$L_{l1} = L_{11} - L_{m1} = L_{11} - \frac{N_1}{N_2} L_{12}, \tag{7}$$

$$L_{l2} = L_{22} - L_{m2} = L_{22} - \frac{N_2}{N_1} L_{21}. \tag{8}$$

Finally, the total leakage inductance on the 1st side can be written as follows:

$$L_{l,total} = L_{l1} + (\frac{N_1}{N_2})^2 L_{l2}. \tag{9}$$

The matrix inductance of studied RTs can be calculated using the magnetostatic as well as finite element simulations. Then, Eqs. (7)-(9) were considered to calculate the total leakage inductance of the studied RTs. Table 2 presents the calculated inductances where the lowest value of the leakage inductance is referred to as RT2 and the worst case (highest value of total leakage inductance) as RT4.

3. Time variant finite element analysis

This section presents the TVFEA of the studied RTs. First, the distribution of employed mesh and magnetic flux density on different volumes of RT is presented in Figure 4(a)-(f). As observed, the maximum flux density is less than 40 mT, hence no saturation in the ferromagnetic parts. The related analysis was done considering the eddy current effect. Here, the employed mesh for all studied configurations is "length-based" with restricted length (the maximum length was set as 0.1 mm) and for the moving parts, "cylindrical-gap-based" moving mesh is considered.

Of note, the presented magnetic flux density is referred to as the TSFEA of the RTs, considering resolver as the load of RTs which has been modeled based on the series RL load ($R = 19\ \Omega$, $L = 2.289$ mH).

Table 2. The inductance values of different RT configurations.

The studied RT	$L_{l,total}$ (nH)	L_{m1} (nH)	$L_{l,total}/L_{m1}$
RT1	90.11	389.28	0.23
RT2	**38.36**	**403.83**	**0.09**
RT3	85.73	402.26	0.21
RT4	110.54	96.79	1.14
RT5	80.08	326.25	0.24
RT6	69.81	189.71	0.37

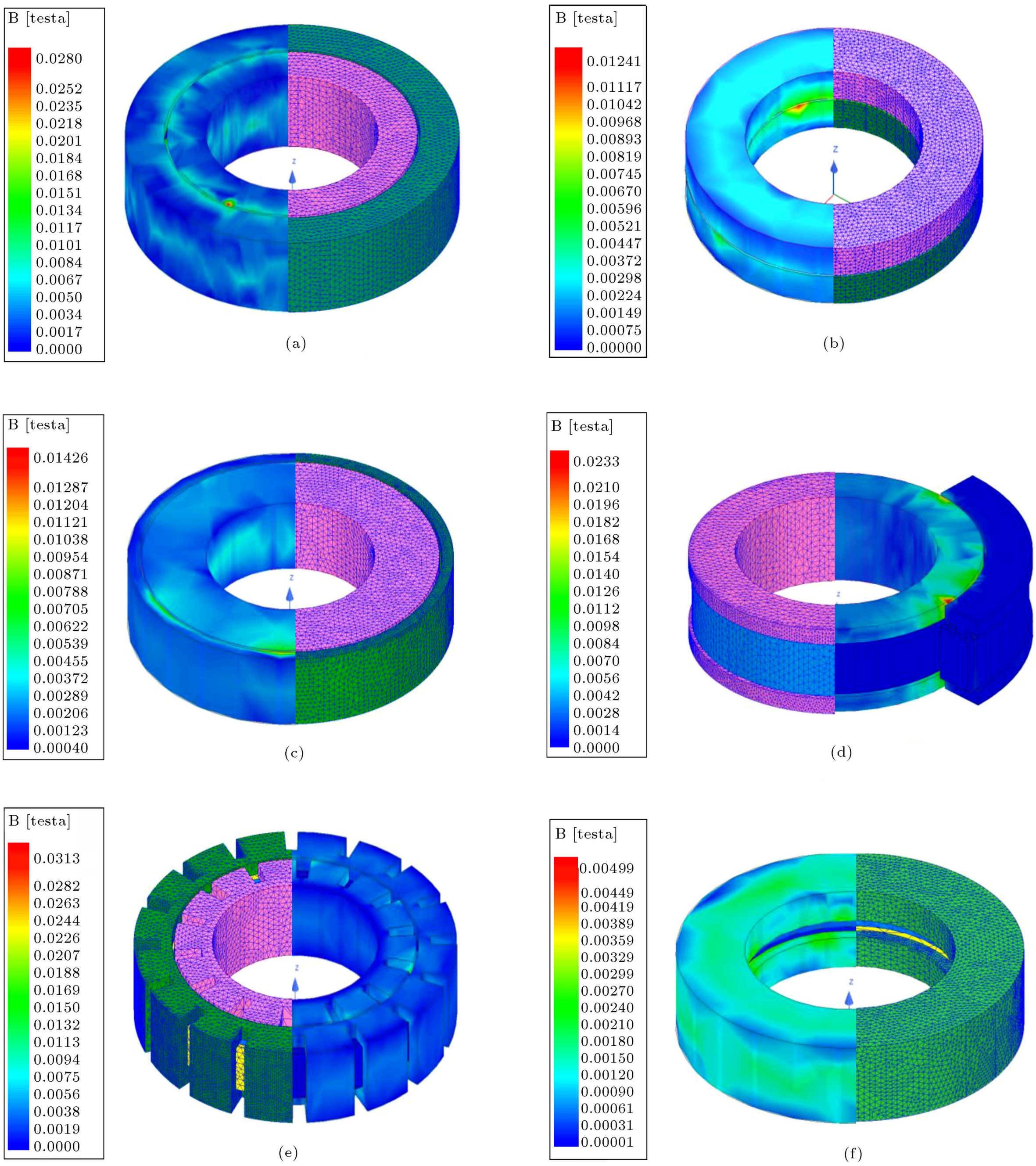

Figure 4. Distribution of the employed mesh and magnetic flux density on the studied RTs: (a) RT1, (b) RT2, (c) RT3, (d) RT4, (e) RT5, and (f) RT6.

Figure 5 shows the no-load induced voltage in the secondary coil at different configurations as well as no-load current. Figure 6 compares the voltage amplitude in the steady state, no-load current amplitude in the steady state, and phase shift error of the induced voltage for different RTs. According to the observations, the maximum/minimum amplitude of the no-load voltage is attributed to RT2/RT4, while the maximum/minimum excitation current is attributed to RT4/RT3. The amplitude of the phase shift error for all the studied RTs is the same, except for RT6 that has the highest phase shift error. Based on the highest ratio of the induced voltage to the excitation current as the index of no-load performance of the RT, RT2 exhibited the best no-load performance among the RTs under study.

The performance of the RTs was evaluated under load conditions in this study. In this regard, two different loads, i.e., resistive ($R = 100$ kΩ) and resistive-inductive (RL), were examined. Both resistance and inductance of the RL load were determined based on the equivalent circuit of a commercial wound-rotor

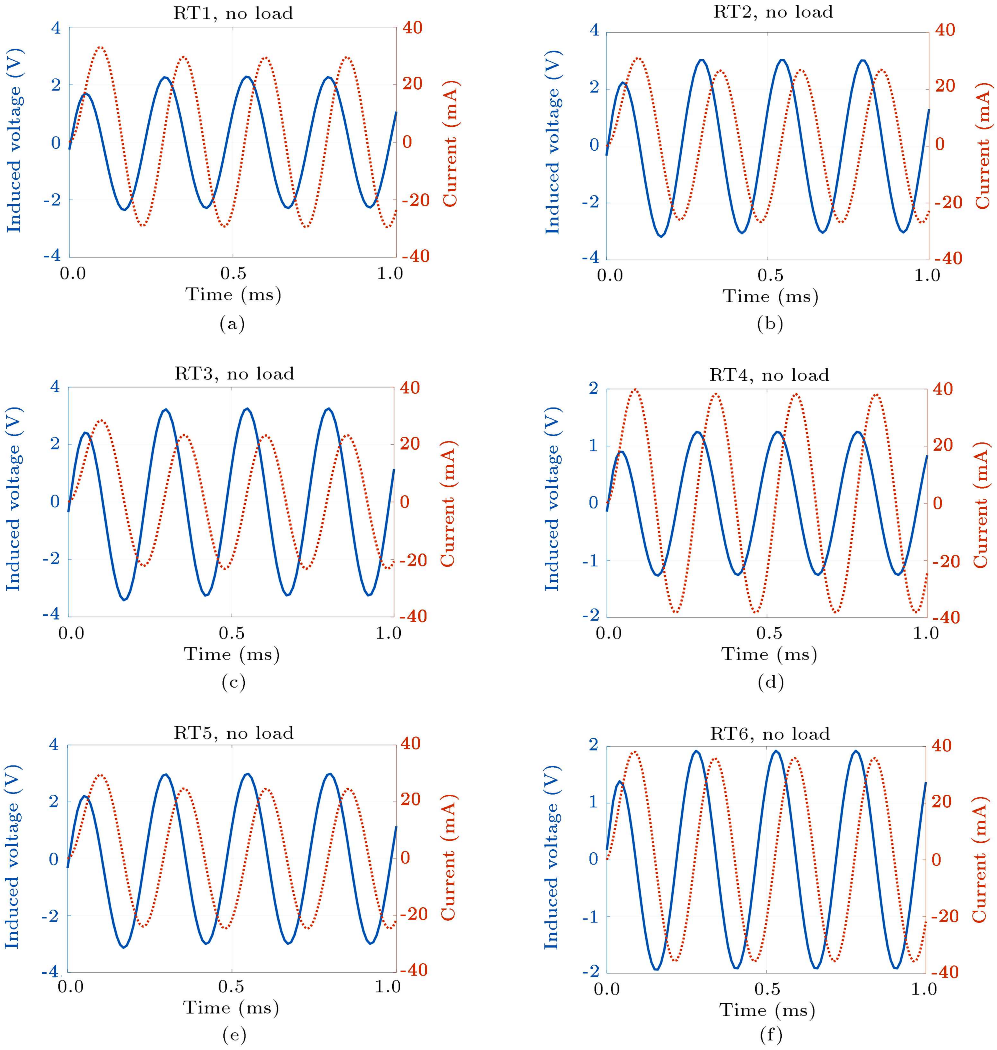

Figure 5. The induced voltage in the secondary coil for different RTs and excitation current in no-load condition: (a) RT1, (b) RT2, (c) RT3, (d) RT4, (e) RT5, and (f) RT6.

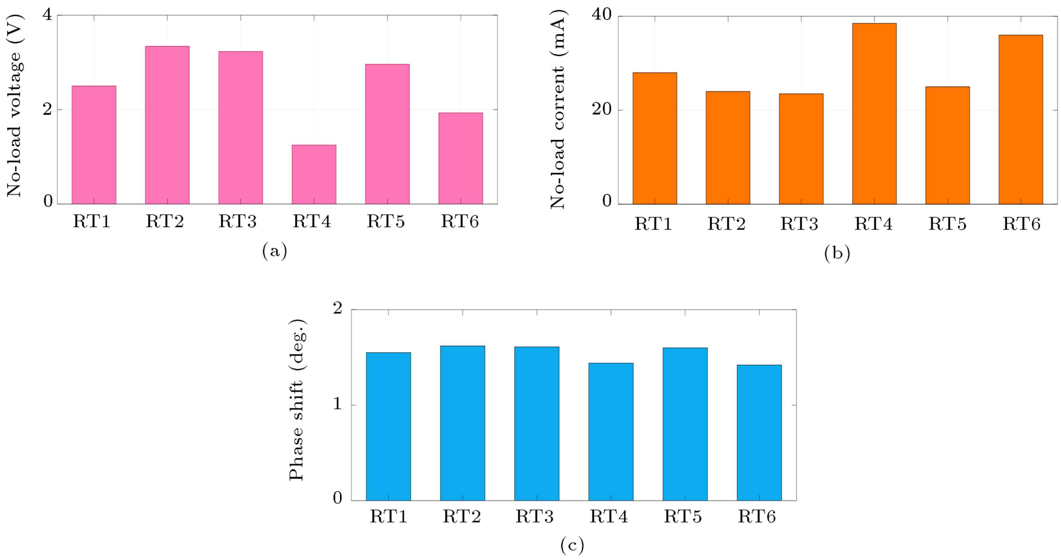

Figure 6. Performance evaluation of different RTs in no-load: (a) Amplitude of the secondary voltage, (b) amplitude of no-load current, and (c) phase shift error.

resolver. Given that the output windings of the resolver are connected to Resolver-to-Digital Converter (RDC) and the input impedance of RDC is extremely high, the output current of the resolver is almost zero. Therefore, the studied resolver can be modeled with resistance (resistance of rotor winding = 19 Ω) in series with inductance that is the series of rotor leakage inductance (0.2 mH) and magnetizing inductance (2.089 mH). Given the excitation voltage of Figure 2, the induced voltage in the secondary coil of different RTs, current of primary coil, and secondary current for R and RL loads are given in Figure 7(a)-(f).

The voltage amplitude in the steady state, primary and secondary current amplitudes in the steady state, and the phase shift error of the induced voltage are compared in Figure 8 for different RTs.

The second RT had the highest amplitude of the induced voltage considering the resolver load (RL load), and RT3 and RT4 had the minimum primary current and minimum phase shift, respectively. The objective function used for selecting RT depends on the type of RT application. For example, in case RT is used for suppling the excitation winding of a resolver, the proper objective function can be defined as:

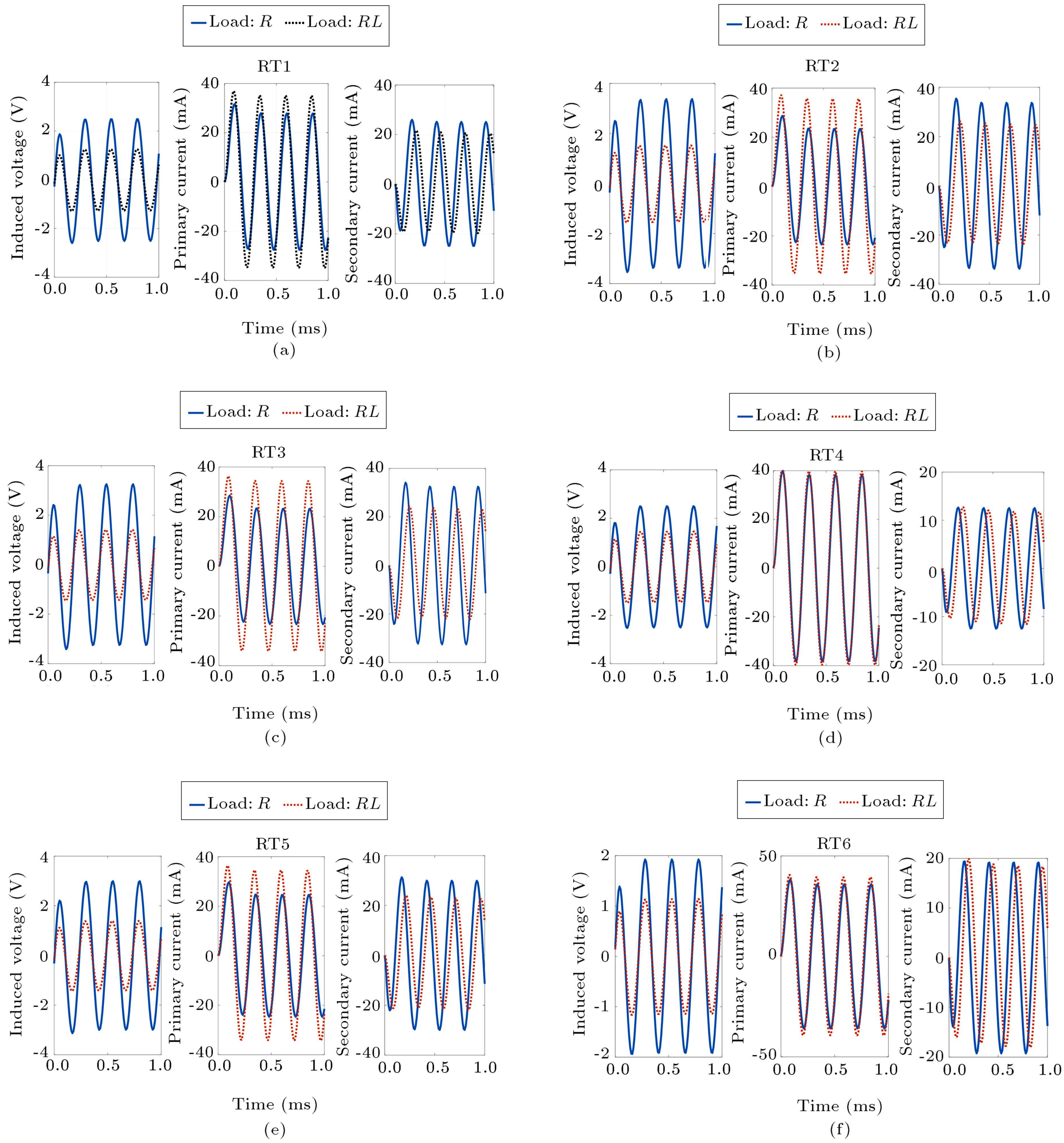

Figure 7. The induced voltage in the secondary coil of different RTs, the primary coil's current, and the current of secondary coil considering R, and RL loads: (a) RT1, (b) RT2, (c) RT3, (d) RT4, (e) RT5, and (f) RT6.

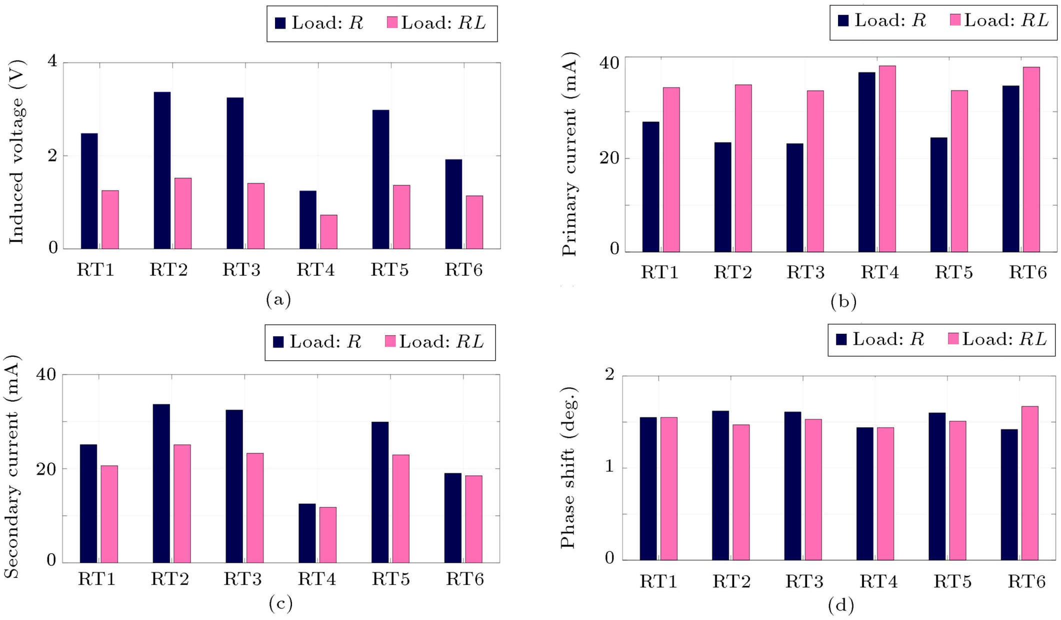

Figure 8. Performance verification of the studied RTs under load condition ($R = 100$ kΩ, RL: $R = 19$ Ω and $L = 2.289$ mH): (a) Amplitude of the induced voltage, (b) amplitude of the primary current, (c) amplitude of the secondary current, and (d) phase shift between the primary and the secondary voltages.

Table 3. Objective function values under different load conditions.

Configuration	O.F.		
	No-load	Under load: R	Under load: RL
RT1	90.8357	89.8975	36.3107
RT2	**140.7867**	**144.7198**	**43.2257**
RT3	139.0568	140.9145	41.5179
RT4	**33.9075**	**33.2290**	**18.9503**
RT5	120.0000	122.8018	40.2510
RT6	55.0311	54.8275	29.4377

$$O.F. = \frac{V_2}{I_1} + \frac{1}{\vartheta}, \tag{10}$$

where V_2 (V) denotes the amplitude of the induced voltage in the secondary coil, I_1 (A) the amplitude of the primary coil current, and ϑ (deg.) the phase shift between the primary and secondary voltages. The lowest phase shift is of significance due to the difficulties associated with the envelope detection of the output signals of the resolver using RDC. The highest value of (10) is achieved using RT2; therefore, RT2 is chosen as the best configuration considering the application of RT along with resolver. Table 3 lists the objective function values at different configurations. As observed in Table 2, the commercial RT, i.e., RT1, exhibits medium performance, while RT2 and RT4 have the worst and best configurations, respectively.

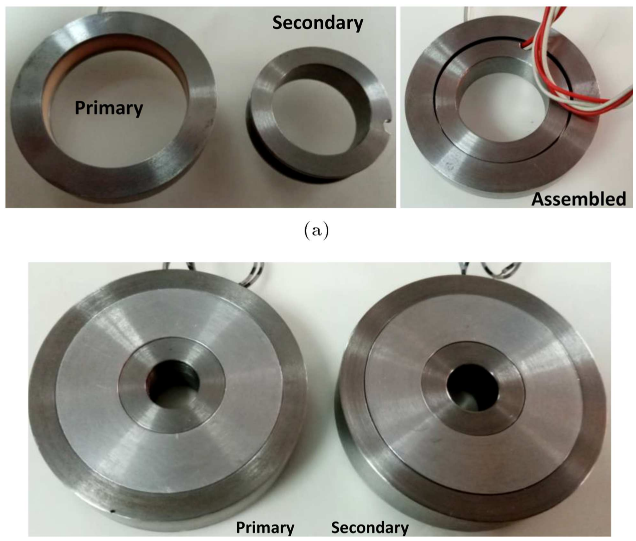

Figure 9. The prototype of RTs: (a) RT1, and (b) RT2.

4. Experimental measurements

With regard to the highest value of the objective function, RT2 is considered as the optimal configuration. Further, the prototype of the commercial RT, i.e., RT1, was also built. The primary and secondary cores were then prototyped, as shown in Figure 9. The

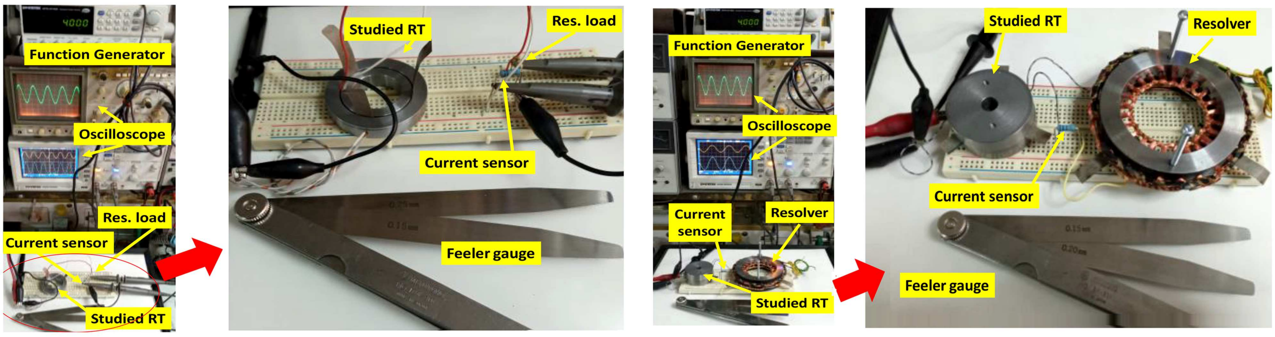

(a) (b)

Figure 10. The test circuit: (a) RT1 with the resistive load and (b) RT2 with resolver load.

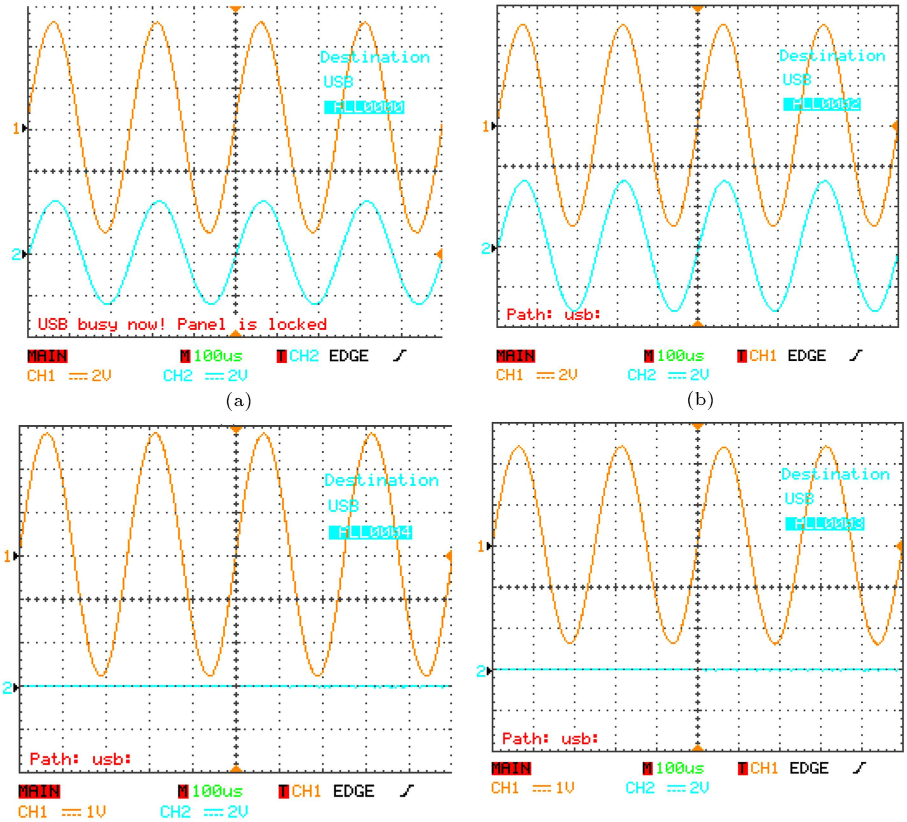

(a) (b) (c) (d)

Figure 11. The experimental results in no-load: (a) Primary and secondary voltages of RT1, (b) primary and secondary voltages of RT2, (c) excitation current of RT1, and (d) excitation current of RT2.

geometrical dimensions of the cores are the same as those of simulated RTs, as demonstrated in Table 1.

Figure 10 presents the test circuit. Table 4 lists the required equipment for the experimental test and their specifications. In the test circuit, the primary coil of the prototype RTs is fed with a 4 kHz sinusoidal voltage using a digital synthesized function generator. The frequency resolution of the employed function generator is 0.1 Hz, and the amplitude of excitation voltage is adjusted using an Automatic Gain Control (AGC) circuit. The induced voltages in the secondary coil in three conditions namely no-load, under $R = 100$ k Ω, and use of a resolver as the load (series RL load: $R = 19\ \Omega$, $L = 2.289$ mH) are sampled and saved using a digital oscilloscope with a sampling rate of 1 GS/sec. A resistive current sensor is then used for measuring the primary and secondary currents. Given that the series RL load is a model of wound rotor resolver, the real wound rotor resolver is used in the experimental test.

Figure 11 presents the test results under the no-load condition. The primary and secondary voltages for RT1 and RT2 are given in Figure 11(a), and (b), respectively. The currents of the primary coil (excitation current of the RTs) for RT1 and RT2 are

Table 4. Specifications of the employed equipment in the experimental setup.

Equipment	Specifications
Prototype RT1 and RT2	Geometrical dimensions according to Table 1
Function generator	Digital synthesized with an automatic gain control (AGC) circuit, The frequency resolution: 0.1 Hz
Digital oscilloscope	Sampling rate: 1 GS/sec
Current sensor	Resistive current sensor
Feeler gauge	Flexible feeler
Resistive load	100 Ω
Resolver as a load	An axial flux disk-type wound rotor resolver

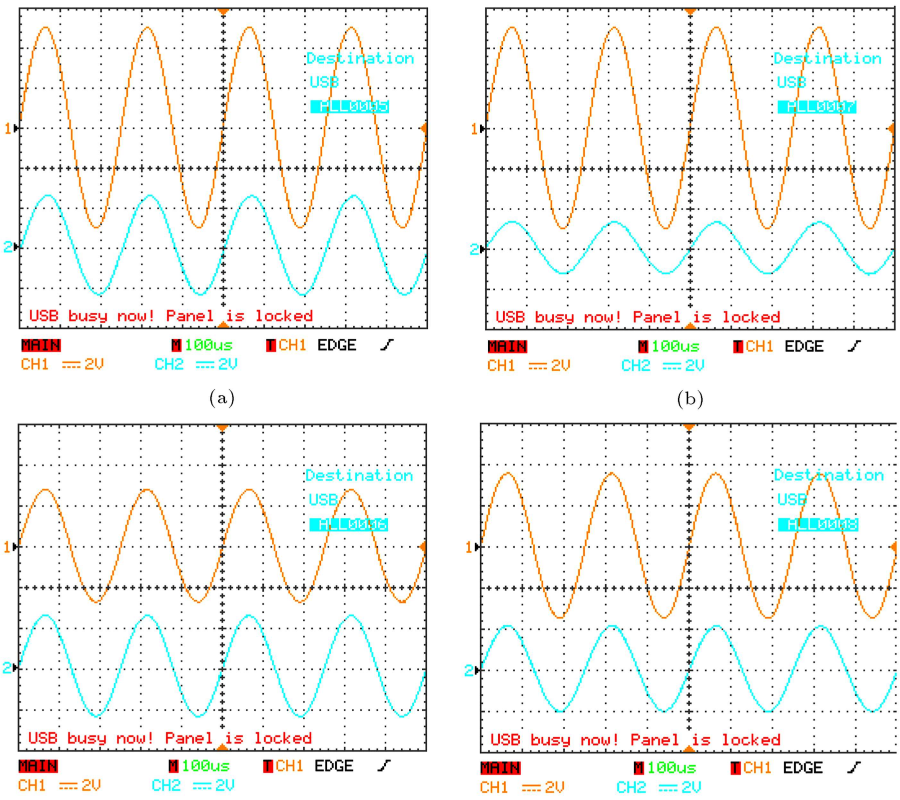

(a) (b) (c) (d)

Figure 12. The experimental results of RT1 under load: (a) Primary and secondary voltages considering $R = 100$ kΩ, (b) primary and secondary voltages considering a resolver as the load, (c) primary and secondary currents considering $R = 100$ kΩ, and (d) primary and secondary currents considering a resolver as the load.

presented in Figure 11(c), and (d), respectively. The measured results of RT1 and RT2 under load conditions are presented in Figures 12 and 13, respectively.

Since the experimental measurements are done in zero speed, the simulations are also repeated in zero speed. As expected, rotating the secondary core of the prototype RTs has no significant impact on the obtained results. Table 5 makes a comparison between the experimental results and simulation ones according to the results of which, in the worst case, the error between the simulation and measured results is less than 7%. The close agreement between the experimental results and those of TVFEM verified the performed simulations.

5. Conclusion

The present research aimed to examine different configurations of rotary transformers. The designed configurations were compared in terms of the induced

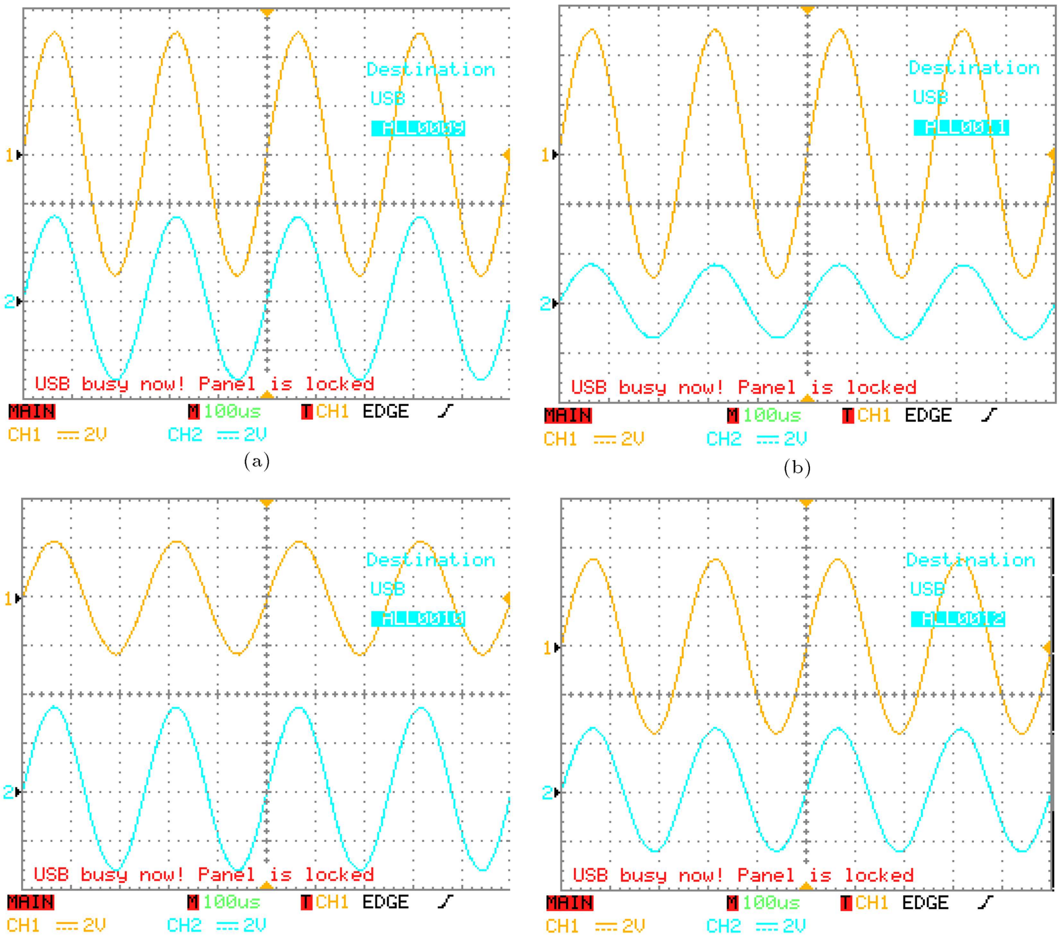

(a) (b) (c) (d)

Figure 13. The experimental results of RT2 under load: (a) Primary and secondary voltages considering $R = 100$ kΩ, (b) primary and secondary voltages considering a resolver as the load, (c) primary and secondary currents considering $R = 100$ kΩ, and (d) primary and secondary currents considering a resolver as the load.

Table 5. Comparison between the measured results and those of TVFEM, considering $V_1 = 5$V, 4 kHz as the excitation voltage of the primary coil.

		RT1				RT2			
		V_2 (V)	I_1 (mA)	I_2 (mA)	ϑ (Deg.)	V_2 (V)	I_1 (mA)	I_2 (mA)	ϑ (Deg.)
No-load	TVFEM	2.50	28	0	1.55	3.34	24	0	1.62
	Measured	2.55	28	0	1.56	3.4	24.5	0	1.63
	|**Error**|%	**1.96**	**0**	**0**	**0.64**	**1.76**	**0.2**	**0**	**0.61**
$R = 100$ kΩ	TVFEM	2.48	27.82	25.11	1.55	3.372	23.4	33.68	1.62
	Measured	2.6	28	26	1.56	3.4	24	34	1.63
	Error%	**4.26**	**1**	**3.42**	**0.64**	**0.82**	**2.5**	**0.94**	**0.61**
Resolver: $R = 19$ Ω, $L = 2.289$ mH	TVFEM	1.25	35.16	20.64	1.55	1.521	35.75	25.09	1.47
	Measured	1.30	36	22	1.58	1.6	36	26	1.50
	|**Error**|%	**3.85**	**2.33**	**6.18**	**1.9**	**4.94**	**6.9**	**3.5**	**2**

voltage amplitude, current of the primary coil, and phase shift error between the primary and secondary voltages. Among the six studied configurations, RT2, the disk-type rotary transformer, exhibited the best performance, while RT4, the segmented primary core RT, had the worst performance. Conventional rotary transformer, RT1, which is the commercially employed with resolvers had an intermediate function. To verify the obtained results, the prototype of the disk-type and commercial RTs were built and tested. Experimental measurements were in agreement with simulated ones.

References

1. Mohammad-Yari, M., Safari, M., Alipour-Sarabi, R., et al. "Optimal winding selection for wound-rotor resolvers", *Scientia Iranica*, **28**(6), pp. 3429–3436 (2021). DOI: 10.24200/sci.2019.52439.2764, early access
2. Lasjerdi, H. and Nasiri-Gheidari, Z. "A comprehensive analysis of short-circuit fault in wound-rotor resolvers", *IEEE Transactions on Vehicular Technology*, **69**(12), pp. 14884–14892 (2020). DOI:10.1109/TVT.2020.3043273.
3. Saneie, H., Nasiri-Gheidari, Z., Tootoonchian, F., et al. "Simplified Winding Arrangement for Integrated Multi-Turn Resolvers", *IEEE Transactions on Industrial Electronic*, **68**(12), pp. 12802–12809 (2020).
4. Bahari, M. and Nasiri-Gheidari, Z. "The comparative analysis of AC-flux and DC-flux resolvers", *Scientia Iranica*, **29**(4), pp. 2007–2013 (2022).
5. Tavakoli, S. and Nasiri-Gheidari, Z. "Static eccentricity fault diagnosis in a cylindrical wound-rotor resolver", *International Journal of Industrial Electronics Control and Optimization*, **3**(1), pp. 19–26 (2020). DOI: 10.22111/ieco.2019.28577.1134
6. Alemi-Rostami, M., Alipour-Sarabi, R., Rezazadeh, G., et al. "Design optimization of a double-stage resolver", *IEEE Transactions on Vehicular Technology*, **68**(6), pp. 5407–5415 (2019). DOI: 10.1109/TVT.2019.2909096.
7. Alipour-Sarabi, R., Nasiri-Gheidari, Z., Oraee, H. "Misconception of total harmonic distortion in resolvers", *Electromechanical Energy Conversion Systems*, **1**(1), pp. 38–43 (2019).
8. Gel, X. and Zhu, Z.Q. "A novel design of rotor contour for variable reluctance resolver by injecting auxiliary air-gap permeance harmonics", *IEEE Transactions on Energy Conversion*, **31**(1), pp. 345–353 (2016).
9. Jing, S., Hao, W., and Weiqiang, W. "The analysis of multipole axial flux reluctance resolver with sinusoidal rotor", 2012 *IEEE 7th International Power Electronics and Motion Control Conference-ECCE Asia*, June 2-5, Harbin, China (2012).
10. Nasiri-Gheidari, Z. "Design analysis, and prototyping of a new wound-rotor axial flux brushless resolver", *IEEE Transaction on Energy Conversion*, **32**(1), pp. 276 –283 (2017).
11. Nasiri-Gheidari, Z. "Investigating the effect of the rotary transformer leakage flux on the detected position of axial flux brushless resolvers", *Tabriz Journal of Electrical Engineering*, **47**(2), pp. 741–749 (2017).
12. Abolqasemi Kharanaq, F., Alipour-Sarabi, R., Nasiri-Gheidari, Z., et al. "Magnetic equivalent circuit model for wound rotor resolver without rotary transformer's core", *IEEE Sensors J.*, **18**(21), pp. 8693–8700 (2018).
13. Tootoonchian, F., Ardebili, M., and Abbaszadeh, K. "Using average DC-pulse response of stator current for identification of single-phase rotary transformer parameters", Przegląd Elektrotechniczny, **88**(11a), pp. 142–146 (2012).
14. Ruviaro M. and Rüncos F. "A brushless doubly fed induction machine with flat plane rotary transformers", *2012 XXth International Conference on Electrical Machines*, Marseille, pp. 23–29 (2012). DOI:10.1109/ICElMach.2012.6349832.
15. Ruviaro, M., Rüncos, F., Sadowski, N. et al. "Design and analysis of a brushless doubly fed induction machine with rotary transformer", *The XIX International Conference on Electrical Machines-ICEM 2010, Rome*, pp. 1–6 (2010). DOI:10.1109/ICELMACH.2010.5607735.
16. Ditze, S., Endruschat, A., Schriefer, T., et al. "Inductive power transfer system with a rotary transformer for contactless energy transfer on rotating applications", *2016 IEEE International Symposium on Circuits and Systems (ISCAS)*, Montreal, QC, pp. 1622–1625 (2016). DOI:10.1109/ISCAS.2016.7538876.
17. Stancu, C., Ward, T., Rahman, K.M., et al. "Separately excited synchronous motor with rotary transformer for hybrid vehicle application", *IEEE Transactions on Industry Applications*, **54**(1), pp. 223–232 (2018)
18. Duan, J., Lina, B., Yang, Q., et al. "Design and testing of a novel rotary transformer for rotary ultrasonic machining", *IEICE Electronics Express*, **14**(23) (2017).
19. Weber, J., Rehfeldt, A., Vip, S., et al. "Rotary transformer with electrical steel core for brushless excitation of synchronous machines", *2016 XXII International Conference on Electrical Machines (ICEM)*, Lausanne, 2016, pp. 884–889 (2016). DOI:10.1109/ICELMACH.2016.7732630.
20. Haruna, J. and Raminosoa, T. "Modeling and steady-state analysis of a rotary transformer-based field excitation system for wound rotor synchronous machine", *2019 IEEE Transportation Electrification Conference and Expo (ITEC), Detroit, MI*, USA, pp. 1–8 (2019). DOI:10.1109/ITEC.2019.8790472.

Biographies

Mehrzad Khazaee received his Bachelor's degree in Power Engineering from Iran Technical and Vocational University (ITVU). He is currently a graduate student of Energy Systems at Iran University of Science and

Technology (IUST). His research interests are electrical machines and renewable energy. He is currently teaching at Shahid Shamsipour Technical College.

Farid Tootoonchian received his BSc and MSc degrees in Electrical Engineering from the Iran University of Sciences and Technology, Tehran, Iran in 2000 and 2007, respectively, and his PhD degree from the K. N. Toosi University of Technology, Tehran, Iran in 2012. He is currently an Associate Professor at the Department of Electrical Engineering, Iran University of Sciences and Technology. His research interests include design, optimization, finite-element analysis, and prototyping of ultrahigh-speed electrical machines, and ultrahigh-precision electromagnetic sensors.